ACS OMEGA

http://pubs.acs.org/journal/acsodf

Article

Electrodeposited PEDOT/Nafion as Catalytic Counter Electrodes for Cobalt and Copper Bipyridyl Redox Mediators in Dye-Sensitized Solar Cells

Edoardo Marchini, Michele Orlandi, Nicola Bazzanella, Rita Boaretto, Vito Cristino, Antonio Miotello, Stefano Caramori, and Stefano Carli*

Cite This: *ACS Omega* 2022, 7, 29181−29194

Read Online

ACCESS | Metrics & More | Article Recommendations | Supporting Information

ABSTRACT: PEDOT-based counter electrodes for dye-sensitized solar cells (DSSCs) are generally prepared by electrodeposition, which produces polymer films endowed with the best electrocatalytic properties. This translates in fast regeneration of the redox mediator, which allows the solar cell to sustain efficient photoconversion. The sustainable fabrication of DSSCs must consider the scaling up of the entire process, and when possible, it should avoid the use of large amounts of hazardous and/or inflammable chemicals, such as organic solvents for instance. This is why electrodeposition of PEDOT-based counter electrodes should preferably be carried out in aqueous media. In this study, PEDOT/Nafion was electrodeposited on FTO and comparatively evaluated as a catalytic material in DSSCs based on either cobalt or copper electrolytes. Our results show that the electrochemical response of PEDOT/Nafion toward Co(II/III-) or Cu(I/II)-based redox shuttles was comparable to that of PEDOT/ClO_4 and significantly superior to that of PEDOT/PSS. In addition, when tested for adhesion, PEDOT/Nafion films were more stable for delamination if compared to PEDOT/ClO_4, a feature that may prove beneficial in view of the long-term stability of solar devices.

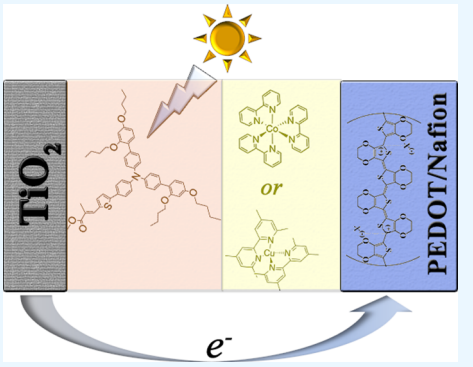

INTRODUCTION

Since the early 1990s, the interest toward dye-sensitized solar cells (DSSCs) has enormously grown owing to the fact that these are the only solar cell devices that can combine photovoltaic performance, easy to scale manufacture, low cost, and transparency.[1,2] DSSCs are capable of converting radiant to electric power with a certified efficiency and a not certified efficiency of 13% and up to 14%, respectively, under standard AM 1.5G (full sun illumination).[3−5] Recently, a new DSSC fabrication approach enabled an improvement of their power conversion efficiency for indoor applications to a record value of 32% under ambient light.[6] Thus, besides constituting a promising photovoltaic platform for outdoor urban and building integration, DSSCs are likely to become in the near future an appealing device for powering indoor applications, such as the internet of things for instance.[7,8] The fulfillment of nowadays record efficiencies has been made possible by focusing the research on the optimization of each of the main parts of the DSSC, that is, the architecture of the photoanode, the sensitizer, the redox mediator, and the catalytic materials at the counter electrode (CE).[9] The CE, in particular, is an essential part of the DSSC, which collects the electrons from the external circuit and regenerates the oxidized redox mediator (Figure 1). In turn, the reduced form of the redox shuttle will diffuse to the photoanode, thereby recovering the oxidized dye generated by the photo-injection of electrons into the mesoporous TiO_2.[2] Thus, the optimal CE accounts for a fast and efficient charge transfer at the interface with the redox couple contained in the electrolyte.

At the beginning of DSSC developments, the most typical catalytic CEs were based on noble metals, in the first place Pt, which offered both high electron transfer rates and high stability in the presence of the iodide/iodine redox mediator. However, platinum was not the optimal electrocatalyst in conjunction with monoelectronic redox couples based on coordination compounds, among which Co(II) and Cu(I) polypyridine complexes are the most successful examples.[10] When used in some Co(II)- and Cu(I)-mediated DSSCs, CEs based on the conductive polymer poly(3,4-ethylenedioxythiophene) (PEDOT) often outperformed platinum, contributing to the achievement of record power conversion efficiencies.[11] From a practical point of view, high performing PEDOT-based CEs are prepared by the electrodeposition method.[11−14] This preparative protocol relies on the electrochemical oxidation of

Received: May 24, 2022
Accepted: July 22, 2022
Published: August 11, 2022

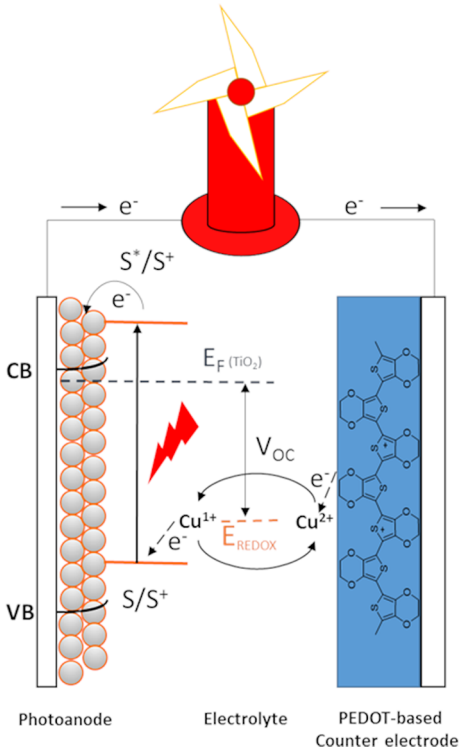

Figure 1. Schematic representation of a DSSC in which the photoanode, a copper-based redox mediator, and a generic PEDOT-based CE are depicted.

the 3,4-ethylenedioxythiophene (EDOT) monomer at FTO (fluorine tin oxide) electrodes in the presence of an appropriate supporting electrolyte. As the PEDOT oligomers grow in size and become insoluble, they deposit on the electrode surface, resulting in the growth of a well-adhered conductive polymeric film on the top of the FTO.[15] Until now, the most efficient PEDOT-based CEs were electrodeposited in the presence of sodium dodecyl sulfate or $LiClO_4$, the former in water solution and the latter in organic media.[12,14] From an applicative point of view, water should be obviously preferred to organic solvents in consideration of environmental benignity, non-flammability, waste management, low cost, and abundance, even more so when scaling up electrode fabrication to large-area conductive supports. A possible drawback that can be linked to the use of monomeric dopants for PEDOT is their intrinsic tendency to be slowly and irreversibly released from the conductive film, especially in the presence of an external electrochemical trigger. This is due to the mechanism of charge transport in PEDOT, which relies on the electrostatic interaction between positive charges in PEDOT and negative charges in the dopant.[16] When electrons/holes are transported across the conductive film, charges moves along PEDOT chains and dopants diffuse to counterbalance charges at different sites, with respect to an initial electroneutral situation. In the presence of an external electrolyte, such as the redox mediator of a DSSC, ion exchange is thus expected between anions in the original PEDOT and those in the electrolyte. This effect is well-understood in the case of drug delivery systems based on conductive polymers, which are known to deliver the negatively charged drugs when cathodic charge is supplied from an external trigger.[17−22] Electron donors in the electrolyte have also been reported to induce this anion exchange in PEDOT doped with tosylate.[23] Due to their steric hindrance, polymeric dopants such as polystyrene sulfonate do not diffuse from the conductive film to the bulk electrolyte. For example, PEDOT doped with polystyrene sulfonate, also known as PEDOT/PSS, is reported to preferably exchange cations rather than anionic polystyrene sulfonate chains.[24] This is because in polystyrene sulfonate, only a fraction of sulfonate groups counterbalance the positive charges in PEDOT, and the others are electrostatically coupled with cations such as sodium or protons, depending on the preparation pathways. Thus, from this perspective, polymeric dopants must be preferred in the DSSC, in order to minimize the possibility that PEDOT CEs release a large number of undesired anions that may alter the composition of the redox mediator, possibly impairing the photovoltaic efficiency of the cell. Nevertheless, CEs based on the well-known PEDOT/PSS, which can be electrodeposited from a water solution of EDOT and sodium polystyrene sulfonate, exhibited a bad kinetic response toward iodide/iodine and alternative redox mediators.[11] Among other water soluble polymeric ionomers, Nafion is one of the most used ion exchange membranes, thanks to its high proton conductivity as well as its large ionic capacitance.[25,26] In this study, for the first time, electrodeposited PEDOT/Nafion films on conductive glass were used to fabricate, in an aqueous environment, CEs for DSSCs. The electrocatalytic activity of these PEDOT/Nafion CEs was explored toward $[Cu(tmbpy)_2]^{2+/+}$ (tmbpy = 4,4′-6,6′-dimethyl-2,2′-bipyridine) and $Co(bpy)_3^{3+/2+}$ (bpy = 2,2′-bipyridine), two of the most popular outer sphere one-electron shuttles for DSSCs.[27−32] The electrochemical response of PEDOT/Nafion (NAF) was comparatively evaluated against that of the benchmark PEDOT/ClO_4 (PER) obtained by electrochemical polymerization in acetonitrile (ACN) and with that of the well-known PEDOT/PSS (PSS) fabricated in water.

RESULTS AND DISCUSSION

The electrochemical oxidation of EDOT at a FTO working electrode, investigated by cyclic voltammetry (CV) either in the presence of $LiClO_4$/ACN or in aqueous Nafion and polystyrene sulfonate sodium salts, is reported in Figure S1. The onset of irreversible oxidation of EDOT is observed at 0.8 V with PSS, at 0.9 V in the presence of Nafion (NAF), and at 1.1 V in ACN/$LiClO_4$ (PER). The presence of two crossing points during the reverse sweep, readily appreciated in the PER electrolyte, is consistent with the nucleation of the polymer on the electrode.[15] The strong dependence of the EDOT oxidation threshold on the supporting electrolyte agrees with the known fact that the oxidation potential of EDOT is cathodically shifted in an aqueous electrolyte, if compared to organic media.[33] In addition, this phenomenon is more pronounced in micellar solutions, thereby suggesting that the oxidation of EDOT is thermodynamically facilitated in the presence of counter ions and/or solvents that provide a better stabilization of EDOT(+) cations.[33] This explains the anticipated oxidation onset of EDOT in NAF and PSS with respect to that in the PER-based monomer solution (see Figure S1). Within the explored conditions, a well-defined diffusional peak associated to the steepest current/voltage of ∼7 mA V^{-1} and the highest Faradaic current is observed with the PER electrolyte, while in aqueous electrolytes, the slope of the voltammograms was significantly lower, on the order of 1 and 0.4 mA V^{-1} for PSS and NAF, respectively, and so is the current density observed at equivalent overvoltages with

https://doi.org/10.1021/acsomega.2c03229
ACS Omega 2022, 7, 29181−29194

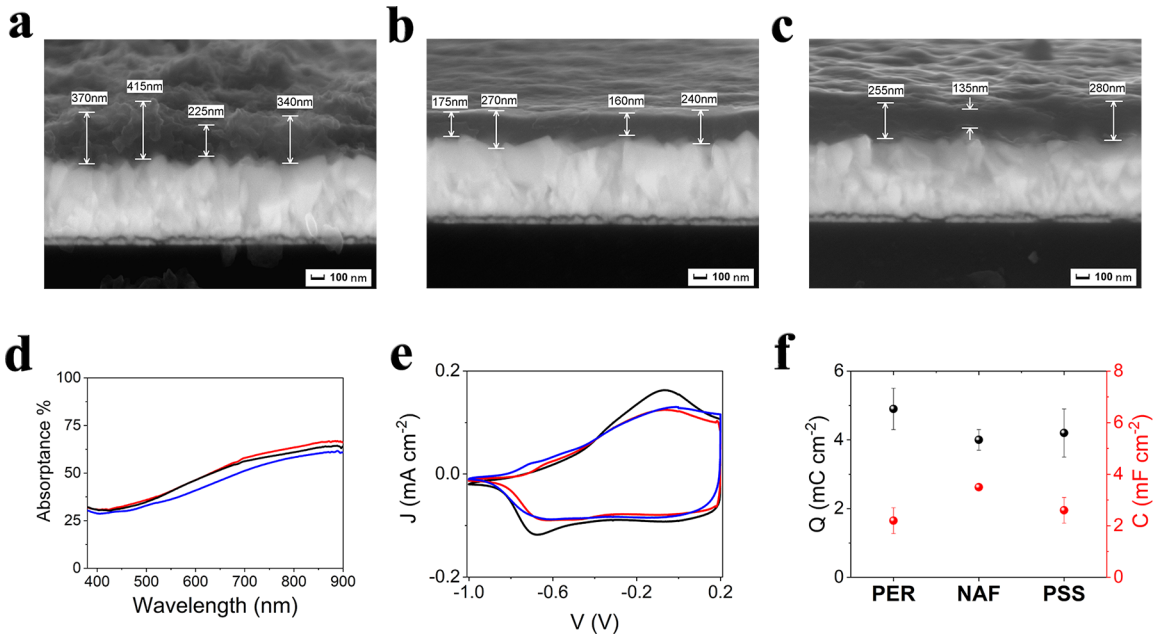

Figure 2. Preliminary characterization of PEDOT-based CEs. (a–c) Cross-section SEM of PER, NAF, and PSS, respectively. (d) Absorptance and (e) CV curves of PER (black), NAF (blue), and PSS (red), showing the neutral to doped transition upon electrochemical cycling. (f) Charge (black dots) extracted from the Faradaic process shown in (e) and capacitances (red dots) obtained from CV curves reported in Figure S3 (data are reported as mean values ± std, n = 3).

respect to the EDOT oxidation threshold (see Figure S1). This behavior might be due to a combination of kinetic and mass transport limitations due to the increased viscosity, and hence resistivity, of the aqueous medium containing bulky polyanions with respect to the small ions contained in the organic PER electrolyte. In addition, a higher resistivity of EDOT/Nafion with respect to that of EDOT/PSS has been reported.[34] Owing to the electrolyte-dependent electrochemical response of EDOT, the potentiostatic electrodeposition conditions were adjusted in each electrolyte in order to properly trigger EDOT oxidation, without intercepting its undesired and detrimental overoxidation of PEDOT, which, particularly in water, is known to occur at a potential higher than 1 V [vs the standard calomel electrode (SCE)].[35] The typical chrono-amperogram recorded in each of the three electrolytes specified above is reported in Figure S2. To ensure a comparable thickness of the electrodeposited PER, NAF, and PSS PEDOT films, we ensured that, in all cases, the same amount of charge (58 mC cm^{-2}) was passed during the electrodeposition. Indeed, it was demonstrated that the thickness of the film, which is linked to the deposited total mass of the polymer coating, is proportional to the amount of the Faradaic charge flowing during the electrodeposition and that the thickness of the film can affect the electrocatalytic properties of the CE and of the resulting solar cell.[12,36,37] Indeed, the obtained PEDOT coatings range between 220 and 340 nm average thickness, as estimated by cross-sectional scanning electron microscopy (SEM) imaging and shown in Figure 2a–c. PER is the thickest and most irregular layer (340 ± 80 nm) and with its very porous and rapidly varying rough morphology yields a varying profile, making it difficult to provide a very reliable thickness estimate. On the other hand, NAF and PSS films display very similar thicknesses (211 ± 52 and 223 ± 77 nm, respectively) and also a much smoother and more compact appearance with respect to PER.

The absorption spectra of PER, NAF, and PSS CEs can be observed in Figure 2d. In particular, the progressive increase of the absorptance from 400 to 900 nm and the absence of any relevant features are consistent with the formation of highly doped PEDOT.[26,38,39] The similar absorptance of the polymer films means that the same amount of the absorbing chromophore is present on the FTO surface, consistent with the equal amount of anodic charge passed during electrodeposition. This also confirms that the thicker appearance of the PER film is probably due to the formation of a highly porous sponge-like PEDOT structure observed in our previous study.[14]

The CV responses of PER, PSS, and NAF films, conducted in an inert electrolyte composed of 0.1 M LiTFSI (TFSI = bis(trifluoromethanesulfonyl)-imide) in ACN, outlined the presence of a cathodic process centered at about −0.65 V, reported in Figure 2e. This process is referred to as the reduction of the conductive film, which reflects the transition from the fully doped and conductive state to the neutral and insulating form of PEDOT.[39] The large separation peak of about 500 mV is consistent with the kinetic limitations for the re-oxidation process probably due to a slow diffusion of ions from the bulk electrolyte to the inner sites of the neutral polymeric film.[40]

Cathodic charge extracted from the CV curves can be used to provide an estimation of the amount of charge carriers in PER, PSS, and NAF CEs, assuming that one electron interacts with each active site of the conductive polymer.[33,36] As depicted in Figure 2f (see also Table S1), quite comparable charges between 4 and 5 mC cm^{-2} are stored in PER, NAF, and PSS CEs, which confirms that the adopted fabrication protocol ensures the injection of a similar amount of charge carriers (holes) into all PEDOT-based CEs. The double layer capacitance, extracted from the capacitive response of the polymer films recorded between 0 and 0.6 V versus SCE (see Figure S3), is slightly larger (≈3.5 mF cm^{-2}) for NAF, whereas

https://doi.org/10.1021/acsomega.2c03229
ACS Omega 2022, 7, 29181−29194

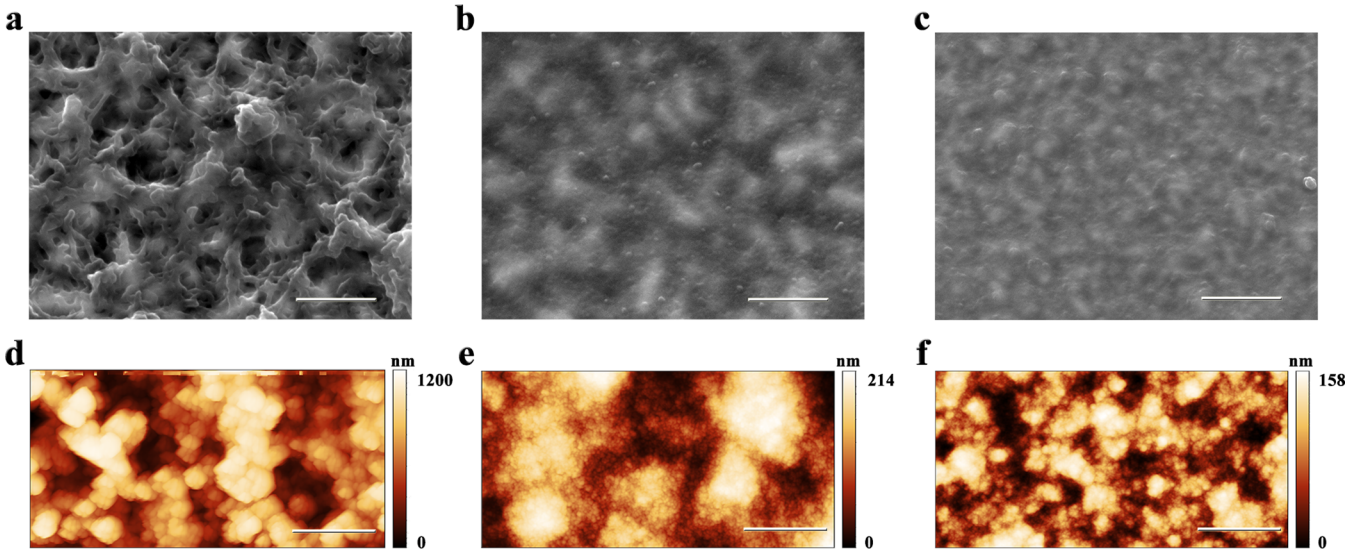

Figure 3. SEM images for (a) PER, (b) NAF, and (c) PSS (scale bar: 500 nm). AFM maps of (d) PER, (e) NAF, and (f) PSS (scale bar: 1 μm).

PER and PSS exhibited a lower value of about 3 mF cm^{-2} (Figure 2f and Table S1). It was reported that NAF films electrodeposited on gold microelectrodes exhibit higher capacitance values if compared to PSS coating prepared in the same conditions. This was mainly ascribed to a faster and more efficient ion diffusion inside the pores of NAF with respect to that in PSS.[34] Thus, it is likely that the good ion transport properties of the ionomer Nafion plays a crucial role in determining the improved capacitance of NAF compared to that of PER and PSS CEs. In addition, it is known that the nature of both the anionic dopant and the solvent used during the electrodeposition strongly affects the surface morphology of the resulting PEDOT films.[13,14,33]

As depicted in Figure 3a–c, SEM top-down imaging reveals a very porous morphology with a sub-micron pore size for PER, while NAF and PSS exhibit more compact surfaces where spherical features with a diameter below 100 nm are visible on the top of the underlying FTO features. This was also corroborated by atomic force microscopy (AFM) analysis, which outlined a porous structure for PER (see Figure 3d), with large pores approximately 300–400 nm wide. This is in line with the sponge-like morphology described in the literature for PEDOT films electrodeposited in organic media and in the presence of small counter ions, such as ClO_4^-.[13,14] Instead, NAF and PSS films are composed of tiny globular substructures, where the nanoglobules's diameter is about 10–20 nm, as shown in Figure 3e,f. This is the typical morphology that is observed when the electrodeposition of PEDOT is carried out in aqueous micellar solutions.[14,34] The highest surface roughness (R_q) of 167 nm was observed for PER, whereas NAF and PSS exhibited a smoother morphology in agreement with SEM imaging (R_q = 38 and 23 nm, respectively), as detailed in Table S2.

The chemical structure of PER, NAF, and PSS films was also evaluated by means of attenuated total reflection–Fourier transform infrared (ATR–FTIR) and Raman spectroscopies. As shown in Figure 4a, FTIR analysis outlined no significant structural differences for PER, NAF, and PSS, and their spectra were dominated by the vibrational signals of the PEDOT backbone. In particular, the bands at 1515, 1290, and 1170 cm^{-1} are linked to the C–C and C=C stretching modes of the

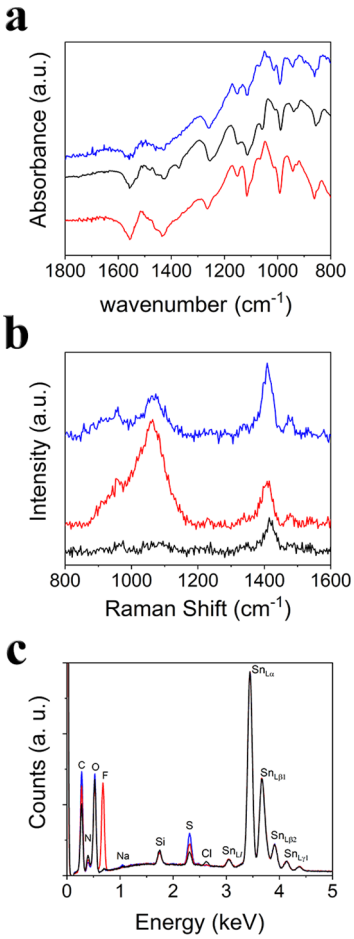

Figure 4. Structural and chemical characterization of PER (black), NAF (red), and PSS (blue) films on FTO: (a) ATR–FTIR spectroscopy, (b) Raman spectroscopy, and (c) EDX.

thiophene ring. The signals at 1080 and 1050 cm^{-1} originate from the vibration mode of the alkylenedioxy group in EDOT. Finally, the bands in the range between 800 and 1000 cm^{-1} can be ascribed to the C–S stretching modes in the thiophene ring.[26]

https://doi.org/10.1021/acsomega.2c03229
ACS Omega 2022, 7, 29181–29194

Raman spectra (Figure 4b) displayed a vibrational peak for all PEDOT-based films at 1414 cm^{-1}, which can be ascribed to the C═C stretching band of highly doped PER, NAF, and PSS polymers.[41] The strong band centered at 1060 cm^{-1}, which is clearly observed in the case of NAF, is ascribed to the stretching mode of $-SO_3^-$ groups in Nafion.[42] As expected, a similar feature is detected also for sulfonate groups in PSS, although in this case, its intensity was less pronounced than that for NAF.[43] It should be noted that in the spectral range of 950−1100 cm^{-1} also, the vibrations of the oxyethylene ring in EDOT are active, giving rise to low intensity peaks near 960 cm^{-1}.[44] The presence of ClO_4^-, Nafion, and polystyrene sulfonate in PER, NAF, and PSS composites was also confirmed by energy-dispersive X-ray spectroscopy (EDX) analysis, as reported in Figure 4c. In particular, PER exhibited a clear Cl peak due to ClO_4^- (Cl 2622 eV $K_{\alpha 1,2}$ peak), while NAF outlined a greatly enhanced fluorine signal (F 677 eV $K_{\alpha 1,2}$ peak) with respect to the small F peak present in PER, which can be linked to the underlying FTO surface. As expected, sulfur is revealed in all samples in the order PER < NAF < PSS, explained by the contribution of the sulfonate groups present in the sulfonate polyanions, which adds to thiophene sulfur in NAF and PSS (S 2307 eV $K_{\alpha 1,2}$ peak).

The electrocatalytic behavior of PER, PSS, and NAF has been investigated in the symmetric thin layer cell (STLC) by means of linear sweep voltammetry (LSV) and electrochemical impedance spectroscopy (EIS), in the presence of either cobalt- or copper-based electrolytes. Herein, the redox mediators are based on the well-known complexes $[Co(bpy)_3]^{2+/3+}$ (Figure 5a) and $[Cu(tmbpy)_3]^{1+/2+}$ (Figure 5b). These redox shuttles, in conjunction with PEDOT-based CEs, enable the fabrication of highly efficient DSSCs.[11]

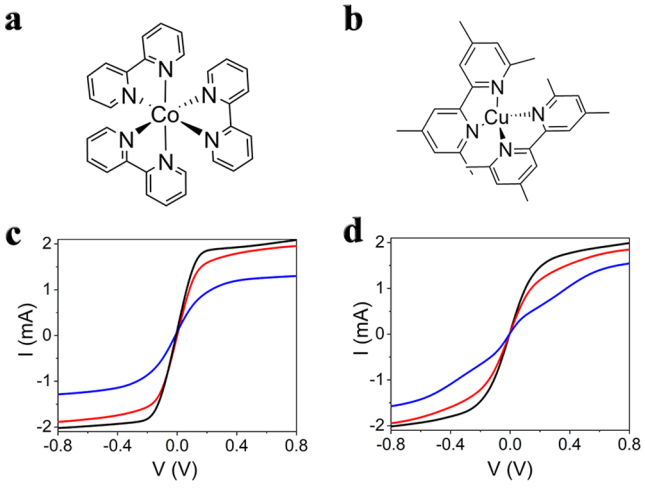

Figure 5. Chemical structure of (a) $[Co(bpy)_3]^{2+/3+}$ and (b) $[Cu(tmbpy)_3]^{1+/2+}$. LSV characterization of dummy cells assembled with (c) $[Co(bpy)_3]^{2+/3+}$- or (d) $[Cu(tmbpy)_3]^{1+/2+}$-based redox mediators, respectively.

The LSV of symmetric cells assembled with PEDOT CEs in conjunction with the $[Co(bpy)_3]^{2+/3+}$ redox mediator exhibits a linear response at low overpotentials, as shown in Figure 5c. The total resistance R_{IV} of the cell can be calculated around the equilibrium potential, according to the Ohm's law $I = (1/R_{IV})\eta$, where I is the current, η is the overpotential, and $(1/R_{IV})$ is the slope of the curve. It should be noted that large values of R_{IV} are originated either by a slow kinetic response at the electrode|electrolyte interface, mass transport limitation, or both.[45] Relatively fast but bulky monoelectronic redox couples such as these polypyridine complexes were predominantly characterized by mass transport limitations even at very low overvoltages (ca. 10 mV). For higher overpotentials, the fully diffusion controlled maximum current I_{lim} (A) is given by eq 1

$$I_{lim} = \frac{2FCDA}{L} \quad (1)$$

where F is the Faraday's constant (96,485 C mol^{-1}), C is the concentration of the redox couple (mol cm^{-3}), D is the diffusion coefficient of the redox species in the electrolyte (cm^2 s^{-1}), L is the thickness of the spacer (cm), and A is the electroactive surface area (ESA) (cm^{-2}).[12,14,46] PER and NAF exhibited comparable R values on the order of 80 Ω in the presence of the $[Co(bpy)_3]^{2+/3+}$ redox mediator, whereas PSS, in the same conditions, yielded the highest total resistance of 170 Ω, as summarized in Table S3. This might account for a faster charge transfer and better mass transport at the interface between the cobalt-based redox shuttle and PER and NAF, if compared to PSS CEs. The poor response of PSS-based CEs in the presence of polypyridine cobalt complexes was already highlighted in a previous study.[14] The highest diffusion limited current of ≈2 mA (8 mA cm^{-2}) was obtained with PER and NAF dummy cells, suggesting that these two materials outline a comparable electrocatalytic activity when used in conjunction with the $[Co(bpy)_3]^{2+/3+}$ redox mediator. In addition, considering that all the parameters in eq 1 are constant, except the term A, the variations of the limiting current can be linked only to the ESA of PEDOT-based CEs. Thus, results are consistent with an improved ESA for PER and NAF with respect to that for the PSS electrodes. This trend is in accordance with the results obtained by AFM analysis, which highlighted a higher roughness for both PER and NAF, which may better expose polymer redox active sites to the electrolyte and also facilitate the diffusion of the redox couple through the porous structure of these materials.

Similar results were obtained for thin cells assembled with the redox shuttle $[Cu(tmbpy)_3]^{+/2+}$, as reported in Figure 5d. Nevertheless, with the $Cu^{+/2+}$ couple, PER exhibited a slightly improved I/V response if compared to that of NAF, as confirmed by the steeper slope of the voltammogram of the former than of the latter, which translates into R_{IV} values of 109 and 128 Ω for PER and NAF, respectively. Also, in this case, PSS outlined the slowest Faradaic response, with a total resistance on the order of 215 Ω. Comparable limiting currents of approximately 2 mA were displayed by PER and NAF in the presence of the $Cu^{2+/+}$ redox shuttle, unlike PSS-based dummy cells, which yielded a lower current of about 1.6 mA. It is interesting to note that larger diffusion coefficients of 11−22 × 10^{-6} cm^2 s^{-1} were reported for $[Cu(tmbpy)_3]^{+/2+}$ than for $[Co(bpy)_3]^{2+/3+}$(6−7 × 10^{-6} cm^2 s^{-1}), and this is not surprising since the diffusion coefficient scales with the hydrodynamical radius of the complex.[27] Thanks to their improved diffusion rate, copper-based redox mediators have been introduced in DSSCs to mitigate the mass transport limitation of cobalt-complex redox electrolytes.[30,32] Now, according to eq 1, one would expect higher diffusional current values for dummy cells assembled with $[Cu(tmbpy)_3]^{+/2+}$ with respect to those with $[Co(bpy)_3]^{2+/3+}$. Thus, the fact that PER and NAF exhibited comparable I_{LIM} values of approximately 2 mA in the presence of both cobalt- and copper-based redox shuttles may seem somehow counterintuitive. This result can

https://doi.org/10.1021/acsomega.2c03229
ACS Omega 2022, 7, 29181−29194

be justified with channel constrictivity effects involving $[Cu(tmbpy)_3]^{+/2+}$ and $[Co(bpy)_3]^{2+/3+}$ diffusing in the PER and NAF porous structure. Indeed, it should be reminded that, unlike conventional 2D metal CEs, where electron transfer occurs entirely at a roughly flat electrode surface, PEDOT is, as a matter of fact, a three-dimensional electrode, being constituted by a relatively porous film, whose pores and voids have electroactive walls and are permeated by the electrolyte. Thus, the redox couple will need to diffuse through the pores of the PEDOT layer before reaching active polymer sites and undergoing electron transfer. Besides geometric constraints, specific interactions between the redox couple, the conductive polymer, and anionic dopants may further affect the local diffusion coefficient of these cationic electronic shuttles within the polymer film. For example, attractive coulombic interaction may result from the negatively charged Nafion and PSS polymer chains and these positively charged metal complexes.

In order to gain more precise information on the electrochemical properties of these PEDOT-based CEs, EIS spectra of the STLCs were collected and fitted to an equivalent circuit model. In Figure 6a,c, the Nyquist and Bode plots,

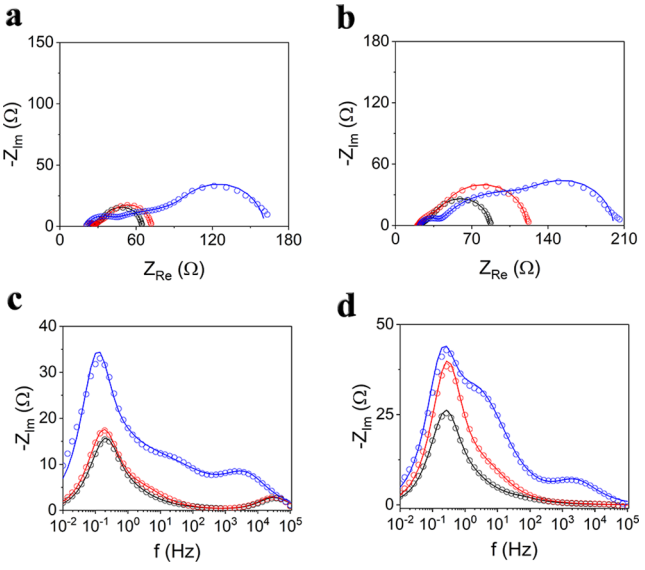

Figure 6. Experimental (circles) and fitted (lines) Nyquist (a,b) and Bode (c,d) plots for dummy cells assembled with (a,c) $Co(bpy)_3]^{2+/3+}$- and (b,d) $[Cu(tmbpy)_3]^{+/2+}$-based redox mediators. The colors black, red, and blue refer to dummy cells fabricated with PER, NAF, and PSS CEs, respectively.

respectively, for PEDOT symmetric cells assembled with $[Co(bpy)_3]^{2+/3+}$ are reported. It can be seen that the Nyquist plots are dominated by a large loop over the low frequency range from ~1 to 0.01 Hz, which is linked to the strong peak at ≈0.1 Hz in the Bode plots. In the high frequency domain, an additional depressed semicircle can be observed (see also Figure S4), with a time constant in the $10^4/10^5$ Hz range for NAF and PER CEs, which shifts to a lower frequency range ($10^3/10^4$ Hz) in PSS (Figure 6c).

The presence of an additional semicircle in the frequency domain of ≈100−10 Hz can be clearly outlined only in the case of PSS, whereas for NAF and PER, this feature is much less evident, although it still produces a shoulder at ca. 10 Hz in the Bode plot of Figure 6c. The shape of the large arc, which dominates the impedance from middle to low frequencies, is indicative of finite transmissive boundary conditions, and it is consistent with the finite-length diffusion behavior.[47] Thus, the equivalent circuit model adopted in this study consists of the serial resistance R_s in series with two parallel (RC) elements, describing the relevant charge transfer processes occurring through the polymer and at the polymer/electrolyte interface. The electric equivalent is reported in Figure S5 and also includes a further finite-length diffusion impedance Z_D to describe the mass transport of the redox couple.[12,14] The impedance Z_D can be expressed by eq 2

$$Z_D = R_D \tanh (j\omega\tau_D)^{1/2}/(j\omega\tau_D)^{1/2} \quad (2)$$

where R_D is the diffusional resistance and τ_D is the diffusional lifetime.[48] To improve the quality of the fitting, two constant phase elements (CPE) were used to model the capacitances. The CPE impedance is given by the relation in eq 3

$$Z_{CPE} = 1/[Y_0(j\omega)^n] \quad (3)$$

where Y_0 is the admittance of the CPE, j is the imaginary unit, ω represents the angular frequency, and n denotes the exponent of the CPE.[48] Referring to the experimental EIS spectra, the highest frequency region contains the contribution of the ohmic resistance R_s, which is due to contact and solution resistance. Comparable R_s values of ≈20 Ω were observed for all CE materials, confirming that this parameter is not affected by the intrinsic conductivity of PEDOT-based coatings but rather by the conductivity of FTO. The highest frequency process was the ion-compensated charge transport inside the porous PEDOT structure, in accordance with the literature, and the circuit element that models its impedance consists of an ion transport resistance (R_{IT}) in parallel with a constant phase element (CPE_{IT}) (Figure S5).[49−52] Interestingly, it was found that this process can be observed for all PEDOT-based CEs assembled with the cobalt mediator, but in the case of copper redox shuttle, it was very noticeable only with PSS, as can be seen in Figure 6d. In contrast, at frequencies higher than 1 kHz, the impedance was frequency independent in the case of PER and NAF dummy cells assembled with the $[Cu(tmbpy)_3]^{+/2+}$-based redox mediator, thereby suggesting that the charge transport resistance across these PEDOT films can be considered negligible for these materials or that the time constant of this process falls at frequencies higher than 10^5 Hz. The fact that this signal is strongly affected by the nature of the electrolyte, rather than by the type of PEDOT, further corroborates the hypothesis that the high frequency process is not simply linked to the charge transfer at the interface FTO||PEDOT, as previously suggested in the literature.[28] In the case of the $[Co(bpy)_3]^{2+/3+}$ redox mediator, a lower value of ion transport resistance was observed for NAF ($R_{IT} \approx 1$ Ω), suggesting that this process is facilitated with this material, if compared to that for PER ($R_{IT} \approx 4$ Ω, see Table S4). The largest values of $R_{IT} \approx 9$ Ω was yielded by PSS to indicate that the ion transport is less efficient in PSS if compared to that in PER and NAF. The charge transfer at the interface PEDOT||$[Co(bpy)_3]^{2+/3+}$ can be observed in the frequency range of ~100−1 Hz.[51] Lower charge transfer resistances R_{CT} of 0.3 and 1.4 Ω were found for PER and NAF, respectively, whereas PSS exhibited the significantly larger R_{CT} value of ≈24 Ω. It is important to note that the charge transfer resistance is directly linked to the heterogeneous electron transfer rate constant k_0.[46] Thus, low values of R_{CT} are desired

https://doi.org/10.1021/acsomega.2c03229
ACS Omega 2022, 7, 29181−29194

to yield fast regeneration of the redox mediator at the CE side in the solar cell device. In this study, an effective charge transfer resistance (R_{CT}) has been considered, in accordance with the literature.[51] This formalism implies that the overall charge transfer resistance must be calculated by considering both the contributions provided by the ion transport resistance (high frequency peak) and the charge transfer resistance (middle frequency semicircle), according to the formula $R_{CT} = R_{IT} + R_{CT}$. Currently, optimal photoanodes can yield short circuit photocurrent values (J_{SC}) of up to 20 mA cm^{-2} at AM 1.5G illumination.[53] This means that a good CE should ensure the generation of comparable exchange currents J_0 at the CE side in order to avoid losses. Assuming a J_{SC} current of 20 mA cm^{-2}, an ideal value of R_{CT} = 1.3 Ω cm^2 can be calculated, according to the relationship in eq 4

$$J_0 = RT/nFR_{CT} \quad (4)$$

where R, T, n, and F are the gas constant, the temperature, the number of electrons, and the Faraday constant, respectively. As summarized in Table S4, NAF and PER yielded the lower R_{CT} values of 0.8 and 1.1 Ω cm^2, respectively, thereby confirming that these two materials can be efficiently used as CEs in a solar cell assembled with the $[Co(bpy)_3]^{2+/3+}$ redox mediator. By contrast, an R_{CT} > 8 Ω cm^2 was obtained for PSS, which would correspond ideally to an exchange current J_0 of ≈3 mA cm^{-2}, making this catalytic material likely unsuitable to be used in conjunction with the $[Co(bpy)_3]^{2+/3+}$ redox shuttle in DSSCs.

As far as the mass transport is concerned, it should be noted that Z_D not only accounts for diffusion processes that occur in the bulk electrolyte but also describes mass transport inside the porous structure of the conductive PEDOT film. This can be clearly understood by considering that PEDOT films is expected to behave like a mixed ionic and electronic electrode. Thus, the highest value of R_D = 73 Ω observed for PSS suggests that ionic diffusion is somehow impeded inside this material. On the other hand, diffusion of $[Co(bpy)_3]^{2+/3+}$ is more efficient through the 3D structure of PER and NAF, as confirmed by their lower R_D values of 35 and 42 Ω, respectively. As reported in Table S4, it can be seen that also the parameter τ_D depends on the catalytic material. The diffusional lifetime can be related to the diffusion coefficient (D) of the redox species by the relationship in eq 5

$$\tau_D = L^2/D \quad (5)$$

where L represents the diffusional length, which in the case of STLCs, was reported to be set as half of the cell spacer (L = 35 μm in this study) .[14] The thickness of the PEDOT film (~300 nm, as discussed above) is negligible with respect to the spacing between the CEs, and we reasonably assume that the whole polymer film is permeated by the electrolyte. L is expected to be constant during dummy cell characterization (35 μm in this study); thus, diffusion coefficients can be extracted from the τ_D values of eq 5 obtained by EIS fittings (Table S4). Increasing diffusion lifetime values of 2.1, 2.2, and 2.7 s were calculated for dummy cells assembled with PER, NAF, and PSS, respectively, in the presence of the $[Co(bpy)_3]^{2+/3+}$ redox mediator. This further confirms that the diffusion of $[Co(bpy)_3]^{2+/3+}$ species is slower inside the porous structure of PSS, if compared to that in PER and NAF. Indeed, the corresponding apparent diffusion coefficients of 5.8, 5.5, and 4.5 × 10^{-6} cm^2 s^{-1} were calculated for PER, NAF, and PSS, respectively. These values are in line with the diffusion coefficients of ≈4.5−6 × 10^{-6} cm^2 s^{-1} reported for $Co(bpy)^{2+/3+}$ for similar electrolyte compositions.[14] The trend here observed can be related to the morphological properties of PEDOT CEs. Indeed, according to AFM analysis (see Table S2), the diffusion of $[Co(bpy)_3]^{2+/3+}$ is expected to be facilitated within the highly open 3D structure of PER (R_q = 167 nm). On the other hand, the more compact surface morphology of PSS (R_q = 23.5 nm) is likely to hinder the diffusion of $[Co(bpy)_3]^{2+/3+}$ complexes. In addition, it is also expected that the bulkier molecular structure of polystyrene sulfonate and Nafion in PSS and NAF, respectively, would translate into a less favored diffusion of $[Co(bpy)_3]^{2+/3+}$ due to a higher steric hindrance and electrostatic interaction between sulfonate groups and hard Co(III) ions if compared to that experienced in the presence of the smaller molecular anion ClO_4^- present inside PER. From this perspective, the most significant difference between polystyrene sulfonate and Nafion can be linked to the presence of the bulkier phenyl rings in the former. This is consistent with previous reports, where the combination of sterically hindered Co(II)/(III) with other, but related, types of PEDOT/PSS electrodes produced very large diffusional resistances and hence a poor electrochemical response.[14]

STLCs assembled with the $[Cu(tmbpy)_3]^{+/2+}$ redox shuttle produced the EIS response reported in Figure 6b,d, with overall features analogous to those just discussed in the case of Co(II)/(III). In the high frequency domain, the semicircle related to the ion transport can be clearly distinguished only in the case of PSS (see Figure S6), with a time constant of ≈3 kHz. A larger charge transfer resistance R_{CT} = 2.4 Ω cm^2 was observed for NAF, if compared to that of PER (R_{CT} = 0.4 Ω cm^2), thereby suggesting that the regeneration of $[Cu(tmbpy)]^+$ is slightly less effective for NAF. Nevertheless, comparable diffusional resistances R_D of 70 and 68 Ω were observed for NAF and PER, respectively, to indicate that the diffusion of the $[Cu(tmbpy)_3]^{+/2+}$ species in NAF is not impaired by the presence of the polymeric ionomer Nafion, with respect to the smaller ClO_4^-. The highest R_{CT} of 12 Ω cm^2 and R_D of 94 Ω were found with PSS, which confirmed that this material is not the best catalytic CE also for the copper-based redox mediator. It was reported that the electrocatalytic properties of Cu-based redox mediators are strongly influenced by the presence of 4-*tert*-butylpyridine (TBP) in the electrolyte. In particular, this additive tends to increase both the charge transfer resistance R_{CT} and the diffusional resistance R_D, if compared to that of a TBP-free redox electrolyte composition.[54] Diffusion lifetimes of 1.5, 1.7, and 1.9 s were extracted from EIS fitting for PER, NAF, and PSS, which translates into diffusion coefficients of 8.2, 7, and 6.4 × 10^{-6} cm^2 s^{-1}, respectively (Table S4). This trend is similar to that observed for PER, NAF, and PSS in conjunction with $[Co(bpy)_3]^{2+/3+}$-based redox mediators, and it is consistent with the AFM analysis, which outlined R_q(PER) > R_q(NAF) > R_q(PSS). It is relevant to observe that the larger values of R_D obtained for $[Cu(tmbpy)_3]^{+/2+}$, if compared to that of $[Co(bpy)_3]^{2+/3+}$ (see Table S4), are indicative of an impaired diffusion of the diffusion-controlling $[Cu(tmbpy)_3]^{2+}$ species, with respect to that of $[Co(bpy)_3]^{3+}$. It is known that upon oxidation to the Cu(II) state, the coordination sphere of $[Cu(tmbpy)_3]^{2+}$ will change from tetrahedral to distorted tetragonal, by coordinating TBP, thereby yielding a larger radius of the complex.[54]

https://doi.org/10.1021/acsomega.2c03229
ACS Omega 2022, 7, 29181−29194

To sum up, STLC characterization confirmed that NAF, deposited in aqueous conditions, rivals the kinetic and mass transport properties of PER and outperforms PSS with both Co(II)/(III) and Cu(I)/(II) electron mediators.

For a possible industrialization, the ideal DSSC device is expected to provide a stable efficient photoconversion over a prolonged time of sunlight irradiation. Several aspects contribute to lowering the DSSC stability, including the dye and TiO_2 degradation, the redox electrolyte chemical changes, evaporation of the solvent and, of course, chemical instability and mechanical detachment of the catalytic material at the CE site. From this point of view, it is known that a possible drawback of PEDOT-based CEs is represented by their tendency to delaminate under mechanical and/or thermal stress. For instance, a protocol to covalently bond PEDOT to the FTO surface was reported, and the resulting films were highly stable to the delamination if compared to conventional PER coatings.[55] Thus, mechanical stability of PER-, NAF-, and PSS-based CEs was monitored by means of a modified scotch tape test. In Figure S7, the images of the CEs before and after the peel off test are shown. As already reported, the as-prepared PER film (Figure S7a) tends to delaminate under these conditions, as confirmed by the presence of several detached areas (Figure S7b). Interestingly, both NAF and PSS displayed an encouraging mechanical stability when subjected to the same mechanical stress test, showing the lack of polymer detachment from the surface (Figure S7c–f). The origin of the improved adhesion of both NAF and PSS is tentatively attributed to the strong interactions of the PEDOT-embedded polyanions, with the hydrophilic surface of FTO, thereby contributing to the increase of the mechanical stability of the conductive polymer film.[26] The stability of PER, NAF, and PSS CEs was also investigated in sealed dummy cells based on the $[Co(bpy)_3]^{2+/3+}$ redox mediator in methoxypropionitrile (MPN), which provides a better long-term stability with respect to ACN. The assembled cells were monitored by LSV at room temperature (RT) during an overall period of 11 days. The two parameters R_{IV} and I_{lim} extracted by LSV were used to evaluate the stability of PEDOT-based CEs. As shown in Figure S8, a strong drop of the current I_{lim} together with an increase of the resistance R_{IV} were observed for PSS after 1 day, suggesting that the kinetic of the charge transfer was impaired at the electrodelelectrolyte interface for this material. NAF and PER exhibited comparable stability under the same conditions, and after ca. 8 days, NAF outperformed PER in terms of the limiting current, showing a slight enhancement with respect to that at day 0. The slope of the NAF i/V curve was also substantially constant during a shelf life of 11 days. This suggests that NAF is a chemically and electrochemically robust catalytic layer, providing a stable electrochemical response within the time window of our experiments.[56]

The electrocatalytic properties of PER, NAF, and PSS CEs were tested in DSSC devices assembled with the organic dye D35. The molecular structure of D35 (see Figure S9) is based on the donor–π–acceptor architecture, and the bulky alkyl chains were introduced on the triphenylamine donor unit to efficiently suppress the photoanode recombination.[57]

The incident photon-to-electron conversion efficiency (IPCE %) and the *JV* characteristics spectra of DSSCs assembled with the $[Co(bpy)_3]^{2+/3+}$ redox mediator are reported in Figure 7a,b, respectively. Relevant DSSC efficiency parameters are summarized in Table 1. As shown in Figure 7a, devices fabricated with PER- and NAF-based CEs exhibited

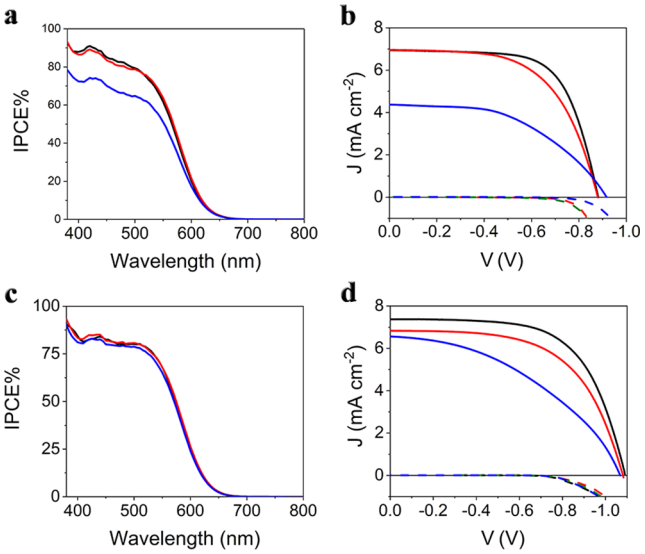

Figure 7. Representative IPCE (a,c) and *J*–*V* (b,d) characteristics of D35-sensitized solar cells assembled with PER, NAF, and PSS CEs and (a,b) $[Co(bpy)_3]^{2+/3+}$ or (c,d) $[Cu(tmbpy)_3]^{+/2+}$ redox mediators at 1 sun of power irradiation. Lines colored in black, red, and blue refer to solar devices assembled with PER, NAF, and PSS CEs, respectively.

comparable photoaction spectra. This translates into similar short-circuit currents (J_{SC}) of ∼7 mA cm^{-2} under *JV* measurements, as depicted in Figure 7b. This is not surprising since J_{SC} scales with IPCE %, and it also relates to the R_{CT} values extracted from dummy cell characterization, as discussed above, which were comparable for CEs based on NAF and PER in conjunction with the cobalt redox mediator.[58] The highest efficiency of ∼4% was obtained for the DSSC fabricated with PER CEs, although solar devices assembled with NAF delivered only slightly inferior performance, exhibiting an efficiency mean value of 3.6%. This was mainly due to a lower fill factor (FF %) of 59 for the DSSC based on NAF if compared to that with PER (FF % = 66). As expected from dummy cell characterization results, solar cells assembled with PSS-based CEs yielded the lowest efficiency η% = 2, which is linked to the smallest values of J_{SC} (4.4 mA cm^{-2}) and FF % = 50. It is interesting to note that the slow kinetic response of PSS CEs, which was also observed during dummy cells analysis (see Table S4), represents a limitation to the photocurrent not only under full sun illumination but also during IPCE measurements, which are typically performed under weaker monochromatic illumination.

In the case of solar cells fabricated with the $[Cu(tmbpy)_3]^{+/2+}$ redox mediator, NAF CEs yielded a lower J_{SC} value of ∼6.8 mA cm^{-2}, if compared to PER (∼7.4 mA cm^{-2}), which may result from the larger R_{CT} exhibited by the former (Table S4), which is consistent with a slower regeneration of the redox mediator and, in turn, of the dye at the photoanode (see Figure 7c,d and Table 1). Overall, the use of NAF instead of PER in otherwise identical cells impacted in a relative 14% decrease in the power conversion efficiency (4.3% for NAF vs 5% for PER), while PSS caused a relative 40% efficiency drop. On the other hand, under the low intensity monochromatic excitation used for IPCE collection, the photoconversion efficiency observed with the $Cu^{+/2+}$ shuttle (IPCE max ≈ 75%) (Figure 7c) was practically independent of the nature of the CE, suggesting that mass transport of the redox couple has a

https://doi.org/10.1021/acsomega.2c03229
ACS Omega 2022, 7, 29181−29194

Table 1. Efficiency Parameters Obtained from the $J-V$ Characterization at 1/0.3 Sun Light Intensity (1 Sun = 100 mW cm^{-2})

CE	redox mediator	intensity (mW cm^{-2})	J_{SC} (mA cm^{-2})	V_{OC} (V)	FF (%)	η (%)
PER	$[Co(bpy)_3]^{2+/3+}$	100	6.9 ± 0.3	0.88 ± 0.01	66 ± 3	4.1 ± 0.3
		30	2.7 ± 0.1	0.77 ± 0.01	69 ± 1	4.9 ± 0.1
NAF		100	6.9 ± 0.4	0.88 ± 0.01	59 ± 3	3.6 ± 0.3
		30	2.5 ± 0.2	0.78 ± 0.01	70 ± 5	4.6 ± 0.1
PSS		100	4.4 ± 0.1	0.91 ± 0.01	50 ± 4	2.0 ± 0.2
		30	2.1 ± 0.1	0.78 ± 0.01	58 ± 1	3.2 ± 0.1
PER	$[Cu(tmbpy)_3]^{+/2+}$	100	7.4 ± 0.3	1.09 ± 0.01	63 ± 2	5.0 ± 0.4
		30	2.85 ± 0.02	1.04 ± 0.01	70 ± 1	6.9 ± 0.1
NAF		100	6.8 ± 0.3	1.08 ± 0.02	59 ± 3	4.3 ± 0.5
		30	2.76 ± 0.02	1.04 ± 0.01	68 ± 3	6.5 ± 0.3
PSS		100	6.6 ± 0.5	1.07 ± 0.02	42 ± 5	3.0 ± 0.5
		30	2.57 ± 0.10	0.99 ± 0.01	42 ± 4	3.5 ± 0.4

big role in determining power conversion under full sun illumination. In order to address this point, we comparatively explored the J/V characteristics of the PEDOT-equipped cells under the reduced irradiance of 30 mW cm^{-2} (0.3 sun) (Table 1 and Figure S10). A general improvement in power conversion efficiency was observed for all cells (Table 1) with the best efficiency (PER) close to 7%. However, also under attenuated illumination, PER confirmed itself as the top material, and it was closely challenged by NAF. For example, with $[Co(bpy)_3]^{2+/3+}$, the efficiency gap between PER and NAF was reduced from 12 to 6% when going from 1 to 0.3 sun, and a similar behavior was observed with $[Cu(tmbpy)_3]^{+/2+}$ (from 14 to 5%). Still, the PSS efficiency continued to lag significantly behind PER and NAF (35 and 49% lower than that of PER with $Co^{3+/2+}$ and $Cu^{+/2+}$ respectively).

The analysis of the efficiency parameters of Table 1 shows that the major impact of the CEs on the current/voltage characteristics of the cell is on J_{SC} and the FF, both of these being strongly linked with the impedance properties of the PEDOT films. V_{OC} is, on the other hand, largely unaffected by the nature of the electrodeposited PEDOT film. V_{OC} is logarithmically dependent on the ratio between the photocurrent and dark current (recombination current) according to the diode equation, eq 6

$$V_{OC} = \frac{kT}{e} \ln \frac{J_{SC}}{J_{dark}} \tag{6}$$

where J_{dark} is the dark current, k is the Boltzmann constant, T is the absolute temperature, and e is the elementary charge.[59,60]

In principle, larger J_{SC} should improve the open-circuit voltage, but more resistive CEs also reduce the dark current J_{dark}, decreasing the overall cell conductivity. This is clearly seen in the lower dark current of PSS/$Co(bpy)_3]^{2+/3+}$ in Figure 7b, which ultimately offsets the decreased J_{SC}, leading to the highest photovoltage among the cobalt-based cells.

The nature of the CE has a major impact on the FF, which incorporates the deviations from the ideality determined by both the shunt and series resistances of the cell. The effect of R_s becomes important under strong direct polarization, that is, when the dark current becomes significant and visibly affects the descending branch of the J/V, from the plateau photocurrent to V_{OC}. R_s sums all the resistive contributions of the cell according to eq 7[61]

$$R_s = R_\Omega + R_T(TiO_2) + R_{CT}(TiO_2) + R_{CT}(CE) + R_D \tag{7}$$

where R_Ω is the constant Ohmic component, $R_T(TiO_2)$ is the transport resistance of TiO_2, $R_{CT}(TiO_2)$ and $R_{CT}(CE)$ are the charge transfer resistances transfer at the photoanode and CE, respectively, and R_D is the diffusional resistance of the redox mediator in the electrolyte.[2] Thus, to address the contribution of the CE to solar cell impedance, we investigated the EIS response of DSSCs fabricated with PER, NAF, and PSS in conjunction with $[Co(bpy)_3]^{2+/3+}$ or $[Cu(tmbpy)_3]^{+/2+}$ mediators. Measurements were carried out under AM 1.5 illumination, and cell impedance was explored at high forward bias, where the electron population of TiO_2 is significant, along the exponential branch of each J/V characteristic. Under these conditions, usually $R_T(TiO_2) < R_{CT}(TiO_2)$ and the transmission line model could be simplified with the circuit model based on two parallel RC elements schematized in Figure S11.[62] To corroborate this choice, we note that no clear rectilinear transmission line features were observed in the high frequency region of complex plane plots. The electric equivalent consists of an Ohmic resistance R_Ω in series with two charge transfer elements and a short Warburg element. The charge transfers occur at the interfaces between the electrolyte and the CE (R_{CE}) or the TiO_2 surface (R_{TiO_2}), respectively, and are described by a charge transfer resistance in parallel with a CPE, to account for the double layer capacitance. The Warburg element (eq 2) describes the electrolyte diffusion through the cell. As reported in Figure S12, the major contribution to the solar cell resistance (the projection of the complex plane arc on the real axis Z_{RE}), which can be readily appreciated from the plots obtained at V_{OC}, is given by the processes occurring in the frequency range of 10 to 10^{-1} Hz, which are linked to the charge transfer at the TiO_2||electrolyte interface (recombination reaction) as well as to the diffusion of the redox shuttle.[14] These processes, in the case of $[Co(bpy)_3]^{2+/3+}$-mediated solar cells fabricated with either PER or NAF CEs give rise to a single depressed semicircle (Figure S12a), resulting from the merging of the charge transfer and short Warburg arcs. These features can be clearly observed by the prominent peak at ≈5 Hz, as depicted in the Bode plots of Figure S12b. In addition to this low frequency feature, PSS exhibits a supplementary depressed semicircle at the higher frequencies of ≈470 Hz, which can be linked to the charge transfer at the CE. As detailed in Table S5, the largest R_{CE} was observed for PSS (110 Ω), whereas for PER and NAF, this parameter was lower than 10 Ω. Comparable charge transfer resistances at the TiO_2||electrolyte interface (R_{TiO_2}) on the range of 55−75 were observed in the

https://doi.org/10.1021/acsomega.2c03229
ACS Omega 2022, 7, 29181−29194

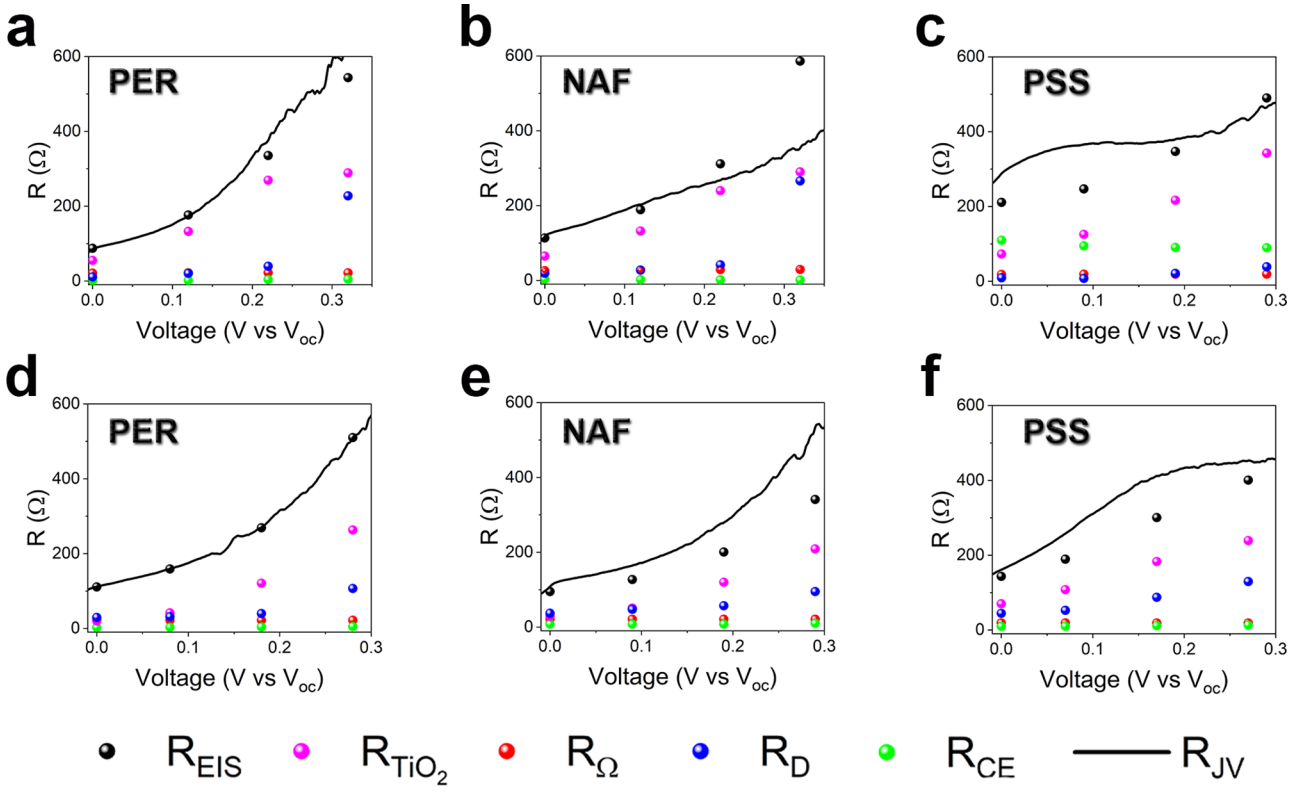

Figure 8. Relevant contributions to cell resistance calculated from EIS measurements in the descending branch of the *JV* curves in Figure 7 (the 0 corresponds to V_{OC}). Dots are resistances extracted from EIS fitting, while the black lines (R_{JV}) are obtained from $\left(\frac{\partial J}{\partial V}\right)^{-1}$ of the *JV* curve.[63] DSSCs assembled with (a–c) cobalt or (d–f) copper redox mediators, where (a–c) and (d–f) refer to PER, NAF, and PSS CEs, respectively.

presence of all CEs, whereas diffusion resistances were found in the interval of 10–20 Ω due to the thinner spacer than that of the TLC. In Figure 8, the most relevant resistive contribution, provided by the fitting model, to the overall impedance was reported by sampling the curve at various bias potentials, with respect to V_{OC}. It is worth noting that the sum of the different contributions, that is, $R_{\Omega} + R_{TiO_2} + R_{CE} + R_D$, is well-aligned with the overall resistance obtained by the inverse of the slope of the *iV* characteristics (see Figure 8a–c), indicating that we have correctly addressed the active elements responsible for photocurrent generation. It is interestingly to note that while the major component to the overall impedance is ascribed to the charge transfer at the TiO_2 interface at all potentials explored, PSS increases substantially the series resistance with a significantly higher R_{CE}, yielding the low FF observed in *i*/*V* curves: in the cases of PER and NAF, the contribution of R_{CE} to R_s was less than 3%, unlike PSS, for which it was higher than 50% and remained quite constant along the potential scan. On the other hand, the diffusion impedance becomes significant only at a higher bias, when the solar cell approaches its limiting current.

Similar features were observed for the EIS analysis of solar cells assembled with the $[Cu(tmbpy)_3]^{+/2+}$ redox mediator, for which, in general, the electron transfer at the interfaces was faster than with the cobalt mediator, generally yielding to the improved FF observed with the former in *i*/*V* curves. In Figure S12c, the Nyquist plots outline the two depressed semicircle related to the TiO_2|electrolyte interface and to the diffusion of the electrolyte, at about 10 and 1 Hz, respectively (see also Figure S12d). The DSSC assembled with PER yielded the lowest R_{CE} (2 Ω), whereas in the cases of NAF and PSS, quite similar values of R_{CE} on the order of 8 and 10 Ω, respectively, were observed. However, in general, for solar cells fabricated with $[Cu(tmbpy)_3]^{+/2+}$, the kinetic contribution of the CE to the overall impedance was not the major one, as can be observed in Figure 8d–f. The trend herein observed for the FF values can be well-explained by considering that both R_{CE} and R_D progressively increased for NAF and PSS, if compared to PER (R_D = 29, 37, and 45 Ω for PER, NAF, and PSS, respectively). Overall PSS has a much better behavior with the $[Cu(tmbpy)_3]^{+/2+}$ couple than with the cobalt electrolyte, but still, within the explored series, generated the most significant contributions to the series resistance of the cell, explaining the lower FF observed when using such a catalytic CE with respect to the other PEDOT-based materials.

CONCLUSIONS

Different PEDOT/polyanion-based CEs were prepared in view of their application as an electrocatalyst in metal complex-mediated solar cells. In particular, we focused on testing PEDOT-based materials that could be obtained via electrodeposition in aqueous conditions as a greener and safer preparative route than relying on organic solvents, which yields, for example, PEDOT/ClO_4. We found that PEDOT/Nafion (NAF), known for its good charge transport properties, can be easily electrodeposited from aqueous media without the need of either tensio-active agents or other additives, to yield sub-micron thick films displaying good mechanical adhesion to FTO and becoming less prone to delamination under mechanical stress than both PEDOT/PSS and PEDOT/ClO_4

https://doi.org/10.1021/acsomega.2c03229
ACS Omega 2022, 7, 29181–29194

films. NAF also exhibited good electrochemical properties toward both cobalt and copper redox mediators. NAF vastly outperforms the electrochemical response of comparable water-processed PEDOT/PSS electrodes, displaying both a lower charge transfer and lower diffusional resistance than the second, and closely challenges the electrochemical performance of PEDOT/ClO_4, known as one of the best reference cathode materials for metal-based DSSCs, particularly under low intensity conditions, where the application of DSSCs shows the most promises. Altogether, these results indicate that PEDOT/Nafion is a promising material for electrocatalytic applications, incorporating also an environmental benefit to the sustainable fabrication of efficient and stable DSSCs.

EXPERIMENTAL SECTION

Materials. 97% EDOT, Alconox, titanium(IV) isopropoxide, magnesium trifluoromethanesulfonate (MgOTf, where OTf = trifluoromethanesulfonate), poly(sodium 4-styrenesulfonate) (NaPSS), 5 wt.% Nafion perfluorinated ion exchange resin solution in a mixture of lower aliphatic alcohols and water, 98% benzimidazole (BzIm), 96% TBP, and solvents (99.8% anhydrous ACN, ACS grade 2-propanol ≥99.8%, ACS grade absolute ethanol (EtOH), 99.9% 1-butanol, andMPN were purchased from Sigma-Aldrich and used without further purification. LiTFSI and 98% nitrosonium tetrafluoroborate ($NOBF_4$) were bought from Alfa Aesar. $LiClO_4$ ≥99% was purchased from Acros organics. FTO TEC-7 was bought from NSG, and 18NR-T TiO_2 paste was purchased from GreatCell Solar. Surlyn 25/50 was supplied by Dyepower Consortium. D35 dye was obtained from Dyenamo. $[Co(bpy)_3](OTf)_2$) and $[Co(II)\ (bpy)_3](PF_6)_3$ were prepared according to a previous work.[64] $[Cu(tmbpy)_2]$TFSI was synthesized according to literature procedures.[27,65]

FTO Cleaning for Electrode Fabrication. Careful cleaning of FTO was carried out by subsequent ultrasonication in 2% w/w aqueous Alconox solution and 2-propanol for 10′ each. After drying at RT, the slides were heated at 450 °C in air in order to burn residual organic contaminants and naturally cooled to RT. The resulting FTO slides were usually employed immediately after completing the cleaning process for electrode fabrication.

PEDOT CEs= Fabrication. 0.25 cm^2 PEDOT-coated CE substrates were prepared by potentiostatic electropolymerization of EDOT on the top of well-cleaned FTO. The same amount of anodic charge (58 mC cm^{-2}) was passed during the electrolysis. A mask made of either Kapton 70 μm or Surlyn 25 μm was used to delimit the exposed FTO geometric area to the value reported above. The electropolymerization was achieved in a three-electrode cell where the FTO working electrode and a 4 cm^2 titanium sheet counter were kept face-to-face at a ca. 2 mm distance from each other, while a double jacket SCE served as the reference electrode. The EDOT solutions and the proper electrodeposition conditions used to prepare the three different PEDOT types are defined as follows (all potentials are in reference to the SCE):

PEDOT/ClO_4 (PER): electrodeposited at 1.6 V from a solution of 10^{-2} M EDOT in 0.1 M $LiClO_4$/ACN. PEDOT/Nafion (NAF): the commercial solution of Nafion (5 % wt) was diluted with water (1:5 v/v, 0.8 % wt), and the pH was adjusted to 6.5−7 with a small amount of diluted $NaOH_{aq}$. The electrodeposition solution was prepared by dissolving EDOT (10^{-2} M) in the neutralized solution of Nafion, and a potential of 1.1 V was used. PEDOT/PSS (PSS): electrodeposition was performed in an aqueous solution of 10^{-2} M EDOT in 0.8% wt. NaPSS at 1 V.

The electrodes for the UV−vis spectroscopy were prepared in a similar fashion by scaling the charge according to the surface area.

STLC Fabrication. These cells were fabricated by clamping two PEDOT electrodes with a 70 μm Kapton spacer. The redox electrolytes were prepared in ACN: (a) 0.18 M $[Co(bpy)_3](OTf)_2$, 0.028 M $[Co(bpy)_3](PF_6)_3$, 0.1 M MgOTf, 0.2 M TBP, and 0.2 M BzIm and (b) 0.208 M $[Cu(tmbpy)_2]$TFSI, 0.028 M $NOBF_4$, 0.1 M LiTFSI, 0.2 M TBP, and 0.2 M BzIm.

The symmetrical TLC employed for the electrochemical stability tests were assembled by sealing two identical PEDOT-based electrodes with 50 μm thick Surlyn. The Co(II)/(III)-based redox mediator was prepared in MPN to guarantee prolonged stability with the formulation reported above and, it was introduced by vacuum backfilling through a small channel on the Surlyn frame. The active area was of 0.25 cm^2. Finally, the channel was sealed with melted Parafilm and epoxy resin to avoid evaporation of the solvent. The STLCs were tested every day, for 11 days, by means of LSV between −1 and +1 V at 20 mV s^{-1} by cycling until the achievement of a steady response.

Solar Cell Fabrication. Photoanodes for solar cells were fabricated as follows: first, a TiO_2 blocking underlayer was fabricated by spin-coating (10″/1000 rpm followed by 20″/2000 rpm) a 0.3 M titanium isopropoxide/butanol solution and sintering in a 500 °C preheated oven for 15′. The porous TiO_2 semiconductor was obtained by spreading the 18NR-T paste on the top of the blocking layer. This was achieved by manually sliding a glass blade on the top of a couple of 3M stripes, acting as spacers, placed at a distance of 5 mm from each other. Sintering of porous TiO_2 was obtained according to the following temperature program: RT−120 °C in 10′, 120−450 °C in 30′, 20′ at 450 °C, 450−500 °C in 10′, and 500 °C for 10 min. After cooling to RT, the resulting electrodes were stained in a 0.2 mM ethanolic solution of D35 overnight, rinsed with fresh ethanol, and dried at RT. Cells were assembled in an open configuration with the aid of two clamps using Surlyn 25 μm as the spacer. Cells were filled with the same electrolytes as those reported for the STLC.

UV/Vis Spectroscopy. Absorption spectra of the various PEDOT-coated FTO electrodes (PER, NAF, and PSS, geometric area = 2.7 cm^2) were registered in the 900−380 nm by evaluating the transmitted (T %) and reflected (R %) light by each substrate type using a JASCO V570 spectrophotometer equipped with an integrating sphere. The spectra are reported as absorptance (A %) versus λ (nm) where $A\ \% = 100\% - T\ \% - R\ \%$.

Infrared and Raman Characterization. ATR−FTIR analysis was performed using a Spectrum 100 FT-IR spectrometer (PerkinElmer Inc., Waltham, Massachusetts, USA) equipped with an ATR accessory (U ATR—1 Reflection Diamond Top plate—ZnSe).

The Raman spectra for the PEDOT films deposited on FTO were acquired using an Edinburgh FS920 spectrofluorimeter equipped with a 189 mW CW 532 nm laser as the excitation source and a photomultiplier tube as the detector. The excitation bandwidth was 0.02 nm, while the emission slit was set at 0.1 nm. 200 scans sampled at a 0.1 nm step were averaged in order to achieve an acceptable S/N ratio.

https://doi.org/10.1021/acsomega.2c03229
ACS Omega 2022, 7, 29181−29194

Scanning Electron Microscopy. SEM was used to analyze the morphology and the thickness of the PEDOT films. Measurements were performed using a JEOL JSM-7001F FEG-SEM at 20.0 keV electron beam energy. The SEM apparatus is equipped with an EDX spectroscopy detector (Oxford INCA PentaFETx3). The working distance was maintained between 3 and 8 mm. Surface morphology images were acquired using secondary electrons in the top-down and tilted mode (Figure 3a−c), whereas cross-sectional analysis was performed by putting the films on a 90° stub and superimposing secondary and backscattering electron images to better separate the film from the FTO substrate (Figure 2a−c). To avoid deformations of the polymer layers, all sample sections were prepared by cutting the glass substrate using a Struers Minitom precision cutting machine, followed by fracturing in liquid nitrogen. A layer of about 20 nm of carbon was then deposited on all samples.

Atomic Force Microscopy. AFM images of the different PEDOT substrates were collected by the aid of a Digital Instruments Nanoscope III scanning probe microscope (Digital Instruments, CA). The instrument was equipped with a silicon tip (RTESP-300 Bruker) and operated in the tapping mode. Surface morphology analysis of raw images was carried out using NanoScope analysis 1.5, and the post-production of the images were carried out using the Gwyddion program.

Electrochemistry. All electrochemical experiments were performed either using an Eco Chemie PGSTAT 302N potentiostat or a PGSTAT30 potentiostat. CV to explore the PEDOT electroactivity on FTO electrodes was performed in a three-electrode setup with a platinum sheet (4 cm^2) CE and a double jacket SCE as the reference. The Faradaic charge (Q) of PEDOT films was calculated by integration of the cyclic voltammograms in the potential range of 0 to −1 V (vs SCE). The capacitances (C) were obtained according to the formula $C = I/\nu$, where I is the current (average of the anodic and cathodic currents at E_{dc}_0.4 V) and ν is the potential scan rate.[66] The voltage was scanned at 20 mV s^{-1} in a 0.1 M LiTFSI/ACN. Polarization curves of the STLCs were obtained at 10 mV s^{-1} in the −0.8 to + 0.8 V range using a two-electrode arrangement. The current/voltage characteristic of each STLC was recorded after a stable voltammetric response (equilibration) of the cell was achieved, testified by the appearance of more than two subsequent superimposable voltammetric curves, established during 20 conditioning cyclic scans between −1 and +1 V. EIS of the equilibrated PEDOT-based STLC was carried out using a PGSTAT 302N equipped with an FRA module by applying a 10 mV sinusoidal perturbation in the 10^5 to 10^{-1} Hz range at 0 V.

Photoelectrochemistry. The density photocurrent−voltage (J−V) curves of 0.25 cm^2 active area DSSCs were obtained using a PGSTAT 302N equipped with an ABET AM 1.5G sun simulator by scanning from the short-circuit voltage (0 V) to the open-circuit voltage (V_{OC}) in the linear sweep mode at a scan rate of 20 mV s^{-1}. Two different irradiance conditions (0.1 and to 0.03 W cm^{-2}) were explored, and each cell was placed on a black opaque platform to avoid backscattered radiation.

IPCE spectra were collected using a home-made apparatus based on a Xe lamp (Ceralux CL300BF) optically coupled with a motorized Newport Cornerstone monochromator.[58] The selected wavelength is focused on the solar cell with an optical fiber. A National Instruments PXI 1033 system was used to acquire the incident irradiance measured using a calibrated photodiode and the photocurrent generated by the solar cells under the short-circuit condition. A black mask bordered the active layer to reduce the contribution of the scattered light from the FTO electrodes and other reflective cell components surrounding the sensitized TiO_2 layer.

■ ASSOCIATED CONTENT

Supporting Information

The Supporting Information is available free of charge at https://pubs.acs.org/doi/10.1021/acsomega.2c03229.

CV, EIS, and J−V characterization (PDF)

■ AUTHOR INFORMATION

Corresponding Author

Stefano Carli − *Department of Environmental and Prevention Sciences, University of Ferrara, 44121 Ferrara, Italy;* orcid.org/0000-0002-0309-2356; Phone: 00390532455415; Email: crlsfn@unife.it

Authors

Edoardo Marchini − *Department of Chemical, Pharmaceutical and Agrarian Sciences, University of Ferrara, 44121 Ferrara, Italy;* orcid.org/0000-0002-8092-1349

Michele Orlandi − *Department of Physics, University of Trento, 38123 Trento, Italy;* orcid.org/0000-0001-5738-3231

Nicola Bazzanella − *Department of Physics, University of Trento, 38123 Trento, Italy*

Rita Boaretto − *Department of Chemical, Pharmaceutical and Agrarian Sciences, University of Ferrara, 44121 Ferrara, Italy*

Vito Cristino − *Department of Chemical, Pharmaceutical and Agrarian Sciences, University of Ferrara, 44121 Ferrara, Italy*

Antonio Miotello − *Department of Physics, University of Trento, 38123 Trento, Italy*

Stefano Caramori − *Department of Chemical, Pharmaceutical and Agrarian Sciences, University of Ferrara, 44121 Ferrara, Italy*

Complete contact information is available at: https://pubs.acs.org/10.1021/acsomega.2c03229

Author Contributions

The manuscript was written through contributions of all authors. All authors have given approval to the final version of the manuscript.

Funding

The University of Ferrara (Italy) acknowledges financial support from the Emilia Romagna Region and H2020 Research Innovation Actions 2020−2024 "CONDOR". This project has received funding from the European Union's Horizon 2020 research and innovation program, under grant agreement no 101006839

Notes

The authors declare no competing financial interest.

■ REFERENCES

(1) O'Regan, B.; Grätzel, M. A Low-Cost, High-Efficiency Solar Cell Based on Dye-Sensitized Colloidal TiO2 Films. *Nature* **1991**, *353*, 737−740.

(2) Muñoz-García, A. B.; Benesperi, I.; Boschloo, G.; Concepcion, J. J.; Delcamp, J. H.; Gibson, E. A.; Meyer, G. J.; Pavone, M.; Pettersson,

H.; Hagfeldt, A.; Freitag, M. Dye-Sensitized Solar Cells Strike Back. *Chem. Soc. Rev.* **2021**, *50*, 12450−12550.
(3) Zhang, D.; Stojanovic, M.; Ren, Y.; Cao, Y.; Eickemeyer, F. T.; Socie, E.; Vlachopoulos, N.; Moser, J. E.; Zakeeruddin, S. M.; Hagfeldt, A.; Grätzel, M. A Molecular Photosensitizer Achieves a Voc of 1.24 V Enabling Highly Efficient and Stable Dye-Sensitized Solar Cells with Copper(II/I)-Based Electrolyte. *Nat. Commun.* **2021**, *12*, 1777.
(4) Zhang, L.; Yang, X.; Wang, W.; Gurzadyan, G. G.; Li, J.; Li, X.; An, J.; Yu, Z.; Wang, H.; Cai, B.; Hagfeldt, A.; Sun, L. 13.6% Efficient Organic Dye-Sensitized Solar Cells by Minimizing Energy Losses of the Excited State. *ACS Energy Lett.* **2019**, *4*, 943−951.
(5) Kakiage, K.; Aoyama, Y.; Yano, T.; Oya, K.; Fujisawa, J. I.; Hanaya, M. Highly-Efficient Dye-Sensitized Solar Cells with Collaborative Sensitization by Silyl-Anchor and Carboxy-Anchor Dyes. *Chem. Commun.* **2015**, *51*, 15894−15897.
(6) Cao, Y.; Liu, Y.; Zakeeruddin, S. M.; Hagfeldt, A.; Grätzel, M. Direct Contact of Selective Charge Extraction Layers Enables High-Efficiency Molecular Photovoltaics. *Joule* **2018**, *2*, 1108−1117.
(7) Michaels, H.; Rinderle, M.; Freitag, R.; Benesperi, I.; Edvinsson, T.; Socher, R.; Gagliardi, A.; Freitag, M. Dye-Sensitized Solar Cells under Ambient Light Powering Machine Learning: Towards Autonomous Smart Sensors for the Internet of Things. *Chem. Sci.* **2020**, *11*, 2895−2906.
(8) Cornaro, C.; Renzi, L.; Pierro, M.; Di Carlo, A.; Guglielmotti, A. Thermal and Electrical Characterization of a Semi-Transparent Dye-Sensitized Photovoltaic Module under Real Operating Conditions. *Energies* **2018**, *11*, 155.
(9) Ye, M.; Wen, X.; Wang, M.; Iocozzia, J.; Zhang, N.; Lin, C.; Lin, Z. Recent Advances in Dye-Sensitized Solar Cells: From Photoanodes, Sensitizers and Electrolytes to Counter Electrodes. *Mater. Today* **2015**, *18*, 155−162.
(10) Wu, J.; Lan, Z.; Lin, J.; Huang, M.; Huang, Y.; Fan, L.; Luo, G.; Lin, Y.; Xie, Y.; Wei, Y. Counter Electrodes in Dye-Sensitized Solar Cells. *Chem. Soc. Rev.* **2017**, *46*, 5975−6023.
(11) Marchini, E.; Caramori, S.; Bignozzi, C. A.; Carli, S. On the Use of PEDOT as a Catalytic Counter Electrode Material in Dye-Sensitized Solar Cells. *Appl. Sci.* **2021**, *11*, 3795.
(12) Ellis, H.; Vlachopoulos, N.; Häggman, L.; Perruchot, C.; Jouini, M.; Boschloo, G.; Hagfeldt, A. PEDOT Counter Electrodes for Dye-Sensitized Solar Cells Prepared by Aqueous Micellar Electrodeposition. *Electrochim. Acta* **2013**, *107*, 45−51.
(13) Xia, J.; Masaki, N.; Jiang, K.; Yanagida, S. The Influence of Doping Ions on Poly(3,4-Ethylenedioxythiophene) as a Counter Electrode of a Dye-Sensitized Solar Cell. *J. Mater. Chem.* **2007**, *17*, 2845−2850.
(14) Carli, S.; Busatto, E.; Caramori, S.; Boaretto, R.; Argazzi, R.; Timpson, C. J.; Bignozzi, C. A. Comparative Evaluation of Catalytic Counter Electrodes for Co(III)/(II) Electron Shuttles in Regenerative Photoelectrochemical Cells. *J. Phys. Chem. C* **2013**, *117*, 5142−5153.
(15) Randriamahazaka, H.; Noël, V.; Chevrot, C. Nucleation and Growth of Poly(3,4-Ethylenedioxythiophene) in Acetonitrile on Platinum under Potentiostatic Conditions. *J. Electroanal. Chem.* **1999**, *472*, 103−111.
(16) Gueye, M. N.; Carella, A.; Faure-Vincent, J.; Demadrille, R.; Simonato, J.-P. Progress in Understanding Structure and Transport Properties of PEDOT-Based Materials: A Critical Review. *Prog. Mater. Sci.* **2020**, *108*, 100616.
(17) Castagnola, E.; Carli, S.; Vomero, M.; Scarpellini, A.; Prato, M.; Goshi, N.; Fadiga, L.; Kassegne, D.; Ricci, S. Multilayer Poly(3,4-Ethylenedioxythiophene)-Dexamethasone and Poly(3,4-Ethylenedioxythiophene)-Polystyrene Sulfonate-Carbon Nanotubes Coatings on Glassy Carbon Microelectrode Arrays for Controlled Drug Release. *Biointerphases* **2017**, *12*, 031002.
(18) Carli, S.; Fioravanti, G.; Armirotti, A.; Ciarpella, F.; Prato, M.; Ottonello, G.; Salerno, M.; Scarpellini, A.; Perrone, D.; Marchesi, E.; Ricci, D.; Fadiga, L. A New Drug Delivery System Based on Tauroursodeoxycholic Acid and PEDOT. *Chem.—Eur. J.* **2019**, *25*, 2322−2329.
(19) Boehler, C.; Asplund, M. A Detailed Insight into Drug Delivery from PEDOT Based on Analytical Methods: Effects and Side Effects. *J. Biomed. Mater. Res., Part A* **2015**, *103*, 1200−1207.
(20) Boehler, C.; Kleber, T.; Martini, M.; Xie, U. G.; Dryg, C.; Martini, N.; Hofmann, I.; Asplund, Y. Actively Controlled Release of Dexamethasone from Neural Microelectrodes in a Chronic in Vivo Study. *Biomaterials* **2017**, *129*, 176−187.
(21) Krukiewicz, K.; Zak, J. K. Conjugated Polymers as Robust Carriers for Controlled Delivery of Anti-Inflammatory Drugs. *J. Mater. Sci.* **2014**, *49*, 5738−5745.
(22) Krukiewicz, K.; Zawisza, P.; Herman, A. P.; Turczyn, R.; Boncel, S.; Zak, J. K. An Electrically Controlled Drug Delivery System Based on Conducting Poly(3,4-Ethylenedioxypyrrole) Matrix. *Bioelectrochemistry* **2016**, *108*, 13−20.
(23) Lindell, L.; Burquel, A.; Jakobsson, F. L. E.; Lemaur, V.; Berggren, M.; Lazzaroni, R.; Cornil, J.; Salaneck, W. R.; Crispin, X. Transparent, Plastic, Low-Work-Function Poly(3,4-Ethylenedioxythiophene) Electrodes. *Chem. Mater.* **2006**, *18*, 4246−4252.
(24) Apraksin, R. v.; Volkov, A. I.; Eliseeva, S. N.; Kondratiev, V. v. Influence of Addition of Lithium Salt Solution into PEDOT:PSS Dispersion on the Electrochemical and Spectroscopic Properties of Film Electrodes. *J. Solid State Electrochem.* **2017**, *21*, 3487−3494.
(25) Mauritz, K. A.; Moore, R. B. State of Understanding of Nafion. *Chem. Rev.* **2004**, *104*, 4535−4586.
(26) Carli, S.; Di Lauro, M.; Bianchi, M.; Murgia, M.; De Salvo, A.; Prato, M.; Fadiga, L.; Biscarini, F. Water-Based PEDOT:Nafion Dispersion for Organic Bioelectronics. *ACS Appl. Mater. Interfaces* **2020**, *12*, 29807−29817.
(27) Saygili, Y.; Söderberg, M.; Pellet, N.; Giordano, F.; Cao, Y.; Muñoz-García, A. B.; Zakeeruddin, S. M.; Vlachopoulos, N.; Pavone, M.; Boschloo, G.; Kavan, L.; Moser, J. E.; Grätzel, M.; Hagfeldt, A.; Freitag, M. Copper Bipyridyl Redox Mediators for Dye-Sensitized Solar Cells with High Photovoltage. *J. Am. Chem. Soc.* **2016**, *138*, 15087−15096.
(28) Tian, H.; Yu, Z.; Hagfeldt, A.; Kloo, L.; Sun, L. Organic Redox Couples and Organic Counter Electrode for Efficient Organic Dye-Sensitized Solar Cells. *J. Am. Chem. Soc.* **2011**, *133*, 9413−9422.
(29) Bignozzi, C. A.; Argazzi, R.; Boaretto, R.; Busatto, E.; Carli, S.; Ronconi, F.; Caramori, S. The Role of Transition Metal Complexes in Dye Sensitized Solar Devices. *Coord. Chem. Rev.* **2013**, *257*, 1472−1492.
(30) Freitag, M.; Giordano, F.; Yang, W.; Pazoki, M.; Hao, Y.; Zietz, B.; Grätzel, M.; Hagfeldt, A.; Boschloo, G. Copper Phenanthroline as a Fast and High-Performance Redox Mediator for Dye-Sensitized Solar Cells. *J. Phys. Chem. C* **2016**, *120*, 9595−9603.
(31) Colombo, A.; Dragonetti, C.; Magni, M.; Roberto, D.; Demartin, F.; Caramori, S.; Bignozzi, C. A. Efficient Copper Mediators Based on Bulky Asymmetric Phenanthrolines for DSSCs. *ACS Appl. Mater. Interfaces* **2014**, *6*, 13945−13955.
(32) Magni, M.; Giannuzzi, R.; Colombo, A.; Cipolla, M. P.; Dragonetti, C.; Caramori, S.; Carli, S.; Grisorio, R.; Suranna, G. P.; Bignozzi, C. A.; Roberto, D.; Manca, M. Tetracoordinated Bis-Phenanthroline Copper-Complex Couple as Efficient Redox Mediators for Dye Solar Cells. *Inorg. Chem.* **2016**, *55*, 5245−5253.
(33) Sakmeche, N.; Aeiyach, S.; Aaron, J. J.; Jouini, M.; Lacroix, J. C.; Lacaze, P. C. Improvement of the Electrosynthesis and Physicochemical Properties of Poly(3,4-Ethylenedioxythiophene) Using a Sodium Dodecyl Sulfate Micellar Aqueous Medium. *Langmuir* **1999**, *15*, 2566−2574.
(34) Carli, S.; Bianchi, M.; Zucchini, E.; Di Lauro, M.; Prato, M.; Murgia, M.; Fadiga, L.; Biscarini, F. Electrodeposited PEDOT:Nafion Composite for Neural Recording and Stimulation. *Adv. Healthcare Mater.* **2019**, *8*, 1900765.
(35) Kamensky, M. A.; Eliseeva, S. N.; Láng, G.; Ujvári, M.; Kondratiev, V. v. Electrochemical Properties of Overoxidized Poly-3,4-Ethylenedioxythiophene. *Russ. J. Electrochem.* **2018**, *54*, 893−901.
(36) Efimov, I.; Winkels, S.; Schultze, J. W. EQCM Study of Electropolymerization and Redox Cycling of 3,4-Polyethylenedioxythiophene. *J. Electroanal. Chem.* **2001**, *499*, 169−175.

https://doi.org/10.1021/acsomega.2c03229
ACS Omega 2022, 7, 29181−29194

(37) Kayinamura, Y. P.; Ovadia, M.; Zavitz, D.; Rubinson, J. F. Investigation of near Ohmic Behavior for Poly(3,4-Ethylenedioxythiophene): A Model Consistent with Systematic Variations in Polymerization Conditions. *ACS Appl. Mater. Interfaces* **2010**, *2*, 2653−2662.
(38) Zozoulenko, I.; Singh, A.; Singh, S. K.; Gueskine, V.; Crispin, X.; Berggren, M. Polarons, Bipolarons, And Absorption Spectroscopy of PEDOT. *ACS Appl. Polym. Mater.* **2019**, *1*, 83−94.
(39) Kvarnström, C.; Neugebauer, H.; Blomquist, S.; Ahonen, H. J.; Kankare, J.; Ivaska, A. In Situ Spectroelectrochemical Characterization of Poly(3,4-Ethylenedioxythiophene). *Electrochim. Acta* **1999**, *44*, 2739−2750.
(40) Ouyang, J.; Xu, Q.; Chu, C. W.; Yang, Y.; Li, G.; Shinar, J. On the mechanism of conductivity enhancement in poly(3,4-ethylenedioxythiophene):poly(styrene sulfonate) film through solvent treatment. *Polymer* **2004**, *45*, 8443−8450.
(41) Chiu, W. W.; Travaš-Sejdić, J.; Cooney, R. P.; Bowmaker, G. A. Studies of dopant effects in poly(3,4-ethylenedi-oxythiophene) using Raman spectroscopy. *J. Raman Spectrosc.* **2006**, *37*, 1354−1361.
(42) Gruger, A.; Régis, A. A.; Schmatko, T.; Colomban, P. Nanostructure of Nafion membranes at different states of hydration. *Vib. Spectrosc.* **2001**, *26*, 215−225.
(43) Stavytska-Barba, M.; Kelley, A. M. Surface-Enhanced Raman Study of the Interaction of PEDOT:PSS with Plasmonically Active Nanoparticles. *J. Phys. Chem. C* **2010**, *114*, 6822−6830.
(44) Nešpůrek, S.; Kuberský, P.; Polanský, R.; Trchová, M.; Šebera, J.; Sychrovský, V. Raman Spectroscopy and DFT Calculations of PEDOT:PSS in a Dipolar Field. *Phys. Chem. Chem. Phys.* **2022**, *24*, 541−550.
(45) Bard, A. J.; Faulkner, L. R. *Electrochemical Methods: Fundamentals and Applications*; J. Wiley & Sons: Hoboken, NJ, 2002.
(46) Liberatore, M.; Petrocco, A.; Caprioli, F.; La Mesa, C.; Decker, F.; Bignozzi, C. A. Mass transport and charge transfer rates for Co(III)/Co(II) redox couple in a thin-layer cell. *Electrochim. Acta* **2010**, *55*, 4025−4029.
(47) Jacobsen, T.; West, K. Diffusion impedance in planar, cylindrical and spherical symmetry. *Electrochim. Acta* **1995**, *40*, 255−262.
(48) Barsoukov, E.; Macdonald, J. R. *Impedance Spectroscopy: Theory, Experiment, and Applications*; John Wiley & Sons, Inc., 2005.
(49) Bianchi, M.; Carli, S.; Di Lauro, M.; Prato, M.; Murgia, M.; Fadiga, L.; Biscarini, F. Scaling of capacitance of PEDOT:PSS: volume vs. area. *J. Mater. Chem. C* **2020**, *8*, 11252−11262.
(50) Danielsson, P.; Bobacka, J.; Ivaska, A. Electrochemical Synthesis and Characterization of Poly(3,4- Ethylenedioxythiophene) in Ionic Liquids with Bulky Organic Anions. *J. Solid State Electrochem.* **2004**, *8*, 809−817.
(51) Kavan, L.; Yum, J. H.; Graetzel, M. Graphene-Based Cathodes for Liquid-Junction Dye Sensitized Solar Cells: Electrocatalytic and Mass Transport Effects. *Electrochim. Acta* **2014**, *128*, 349−359.
(52) Roy-Mayhew, J. D.; Bozym, D. J.; Punckt, C.; Aksay, I. A. Functionalized Graphene as a Catalytic Counter Electrode in Dye-Sensitized Solar Cells. *ACS Nano* **2010**, *4*, 6203−6211.
(53) Stojanović, M.; Flores-Diaz, N.; Ren, Y.; Vlachopoulos, N.; Pfeifer, L.; Shen, Z.; Liu, Y.; Zakeeruddin, S. M.; Milić, J. v.; Hagfeldt, A. The Rise of Dye-Sensitized Solar Cells: From Molecular Photovoltaics to Emerging Solid-State Photovoltaic Technologies. *Helv. Chim. Acta* **2021**, *104*, No. e2000230.
(54) Kavan, L.; Saygili, Y.; Freitag, M.; Zakeeruddin, S. M.; Hagfeldt, A.; Grätzel, M. Electrochemical Properties of Cu(II/I)-Based Redox Mediators for Dye-Sensitized Solar Cells. *Electrochim. Acta* **2017**, *227*, 194−202.
(55) Carli, S.; Casarin, L.; Bergamini, G.; Caramori, S.; Bignozzi, C. A. Conductive PEDOT Covalently Bound to Transparent FTO Electrodes. *J. Phys. Chem. C* **2014**, *118*, 16782−16790.
(56) Kamppinen, A.; Aitola, K.; Poskela, A.; Miettunen, K.; Lund, P. D. Stability of Cobalt Complex Based Dye Solar Cells with PEDOT and Pt Catalysts and Different Electrolyte Concentrations. *Electrochim. Acta* **2020**, *335*, 135652.
(57) Feldt, S. M.; Gibson, E. A.; Gabrielsson, E.; Sun, L.; Boschloo, G.; Hagfeldt, A. Design of Organic Dyes and Cobalt Polypyridine Redox Mediators for High-Efficiency Dye-Sensitized Solar Cells. *J. Am. Chem. Soc.* **2010**, *132*, 16714−16724.
(58) Hagfeldt, A.; Boschloo, G.; Sun, L.; Kloo, L.; Pettersson, H. Dye-Sensitized Solar Cells. *Chem. Rev.* **2010**, *110*, 6595−6663.
(59) Peter, L. M. Dye-Sensitized Nanocrystalline Solar Cells. *Phys. Chem. Chem. Phys.* **2007**, *9*, 2630−2642.
(60) Adachi, M.; Sakamoto, M.; Jiu, J.; Ogata, Y.; Isoda, S. Determination of Parameters of Electron Transport in Dye-Sensitized Solar Cells Using Electrochemical Impedance Spectroscopy. *J. Phys. Chem. B* **2006**, *110*, 13872−13880.
(61) Qi, B.; Wang, J. Fill Factor in Organic Solar Cells. *Phys. Chem. Chem. Phys.* **2013**, *15*, 8972−8982.
(62) Fabregat-Santiago, F.; Bisquert, J.; Garcia-Belmonte, G.; Boschloo, G.; Hagfeldt, A. Influence of Electrolyte in Transport and Recombination in Dye-Sensitized Solar Cells Studied by Impedance Spectroscopy. *Sol. Energy Mater. Sol. Cells* **2005**, *87*, 117−131.
(63) Fabregat-Santiago, F.; Bisquert, J.; Palomares, E.; Otero, L.; Kuang, D.; Zakeeruddin, S. M.; Grätzel, M. Correlation between Photovoltaic Performance and Impedance Spectroscopy of Dye-Sensitized Solar Cells Based on Ionic Liquids. *J. Phys. Chem. C* **2007**, *111*, 6550−6560.
(64) Cazzanti, S.; Caramori, S.; Argazzi, R.; Elliott, C. M.; Bignozzi, C. A. Efficient Non-Corrosive Electron-Transfer Mediator Mixtures for Dye-Sensitized Solar Cells. *J. Am. Chem. Soc.* **2006**, *128*, 9996−9997.
(65) Kelly, N. R.; Goetz, S.; Batten, S. R.; Kruger, P. E. Coordination behaviour and network formation with 4,4′,6,6′-tetracarboxy-2,2′-bipyridine and 4,4′-dicarboxy-2,2′-bipyridineligands with rare and alkaline earth metals. *CrystEngComm* **2008**, *10*, 68−78.
(66) Tanguy, J.; Mermilliod, N.; Hoclet, M. Capacitive Charge and Noncapacitive Charge in Conducting Polymer Electrodes. *J. Electrochem. Soc.* **1987**, *134*, 795−802.

https://doi.org/10.1021/acsomega.2c03229
ACS Omega 2022, 7, 29181−29194